Journal of Simulation & Analysis of Novel Technologies in Mechanical Engineering
12 (4) (2019) 0019~0040
HTTP://JSME.IAUKHSH.AC.IR
ISSN: 2008-4927

Analysis of Stress Intensity Factors in Hollow Cylinders Reinforced by an Effective Coating Containing Multiple Cracks

Mostafa Karimi [1,*], Alireza Hassani [2]

1- Young Researchers and Elites Club, Fereydan Branch, Islamic Azad University, Isfahan, Iran
karimidarani@gmail.com

2- Young Researchers and Elites Club, Science and Research Branch, Islamic Azad University, Tehran, Iran
ahassani1111@gmail.com

(Manuscript Received --- 25 Jul. 2019; Revised --- 12 Sep. 2019; Accepted --- 16 Nov. 2019)

Abstract

In this paper, the solution of an isotropic hollow cylinder, with an isotropic coating, weakened by multiple radial cracks is studied. The hollow cylinder and its coating are under Saint-Venant torsional loading. The series solution is then derived for displacement and stress fields in the cross section of the cylinder containing a Volterra-type screw dislocation. The dislocation solution is employed to derive a set of Cauchy singular integral equations for the analysis of multiple curved cracks. The solution to these equations is used to determine the torsional rigidity of the domain and the stress intensity factors (SIFs) for the tips of the cracks. Finally, several examples are presented to show the effect of the coating on the reduction of the mechanical stress intensity factor in the hollow cylinder.

Keywords: Saint-Venant torsion; several cracks; isotropic coating; Stress intensity factor; Distribution dislocation technique; Torsional rigidity

1- Introduction

Shafts in a machine are bars to hold or turn other parts that move or spin. Due to simplicity of manufacturing, they are generally produced in the form of the bars with circular cross-section. Shafts are often subjected to torsion in the process of working; therefore cracking is one of their major issues. Therefore, it is important to examine the shafts from the point of view of fracture mechanics. Though the torsion problem of a hollow cylinder is rather old in the theory of elasticity, but the effect of coating structure on stress intensity factors in a hollow cylinder with multiple cracks has not been adequately developed at present time.

The problems of elastic cylindrical shafts under torsional loading have been investigated by numerous researchers. In order to review torsion problems, it is convenient to categorize them into two major groups: those primarily dealing domains without any crack, and those studying shafts contained with single or several cracks. Within the first category, number of researchers has studied torsion problems in the intact bars [1-4].

There are other investigations studying the shafts with single or several cracks which

the shafts with multiple arbitrary oriented curved cracks have not been developed sufficiently. The defects in the following papers were assumed to be extended throughout the shaft axis. At the first we review the shafts with circular cross section.

The complete analysis of the torsional rigidity of a solid cylinder with radial cracks was obtained by Lebedev et al. [5]. The authors investigated the problem of the twisting of an elliptical cross section containing two edge cracks extending to its foci. Xiao-chun and Ren-ji [6] presented an analytical solution for a solid cylinder weekend by a screw dislocation. The problem was reduced to solve a singular integral equation for the unknown dislocation density with aid of the dislocation distribution technique. The stress intensity factor and torsional rigidity were calculated by solving the ensuing singular integral equation numerically.Torsion analysis of a hollow cylinder with an orthotropic coating containing several cracks were done. A formulation for a hollow cylinder weakened by cracks with an orthotropic coating was presented by Karimi, et al. [7].Analysis of a solid cylinder with the curvilinear cracks subjected to Saint-Venant torsion was treated by Wang and Lu [8]. With aid of the boundary element method, the authors evaluated boundary integral equations only on the cracks surfaces. Also, stress intensity factor of the crack tip and torsional rigidity were determined for a straight, kinked or eccentric circular-arc crack. The analysis of the hollow cylinder with four edge cracks normal to the inner boundary of the cylinder under torsion was the subject of study done by Chen [9]. The author made use of a method similar to that used in reference [8]. The problem was reduced to a Dirichlet problem of the Laplace equation and evaluated with help of the finite difference method. Finally, the stress intensity factors of the crack tips and the torsional rigidity were calculated numerically. Tweed and Rooke [10] analyzed the Saint-Venant torsion problem of a circular cross section with containing a symmetric array of edge cracks. By symmetry, the problem reduced an integral equation to that of finding the warping functions in some sectors. Finally, the stress intensity factor and crack energy were computed by solving the ensuing integral equation.Yuanhan [11] studied problem of a thick-walled cylinder with a radial edge crack under torsional loading. An expansion for the stress function was employed so that the resultant stresses to have the square root singularity at the crack tip. The unknown coefficients of the expansion were calculated by boundary collocation method. At the end, the torsional rigidity of the thick-walled cylinder and the stress intensity factor of crack tip were achieved.Chen et al. [12] analyzed a circular cross section bar weekend by a straight edge crack under Saint-Venant torsion with aid of dual boundary element method. The authors indicated that the dual boundary element method provides excellent accuracy and simplifies the modeling. The dual boundary element method involved modeling only on the boundary without considering the artificial boundary as the multi-zone method. The domain cell was not discretized, since the domain of the integral for calculation of the torsion rigidity was divided into two boundary integrals by means of the Green’s second identity and Gauss theorem.The problem

of an orthotropic bar with circular cross section under Saint-Venant torsion was treated by Hassani and Faal [13]. The solution of a Volterra-type screw dislocation was first obtained with aid of a finite Fourier cosine transform. Next, the dislocation solution was employed to derive a set of Cauchy singular integral equations for analysis of the bar with multiple cracks. Chen [14] studied a hollow bars with outer or inner keys under torsion by the harmonic function continuation technique and conformal mapping. Fang-ming and Ren-ji [15] addressed the torsion problem of a circular bar weekend by internal crack that reinforced by a ring of rod, made of different material of the cylinder. By means of the Muskhelishvili single-layer potential function solution and the single crack solution for the problem of a cylinder under Saint-Venant torsion, the problem was reduced to a set of mixed-type generalized Cauchy singular integral equation. The analysis for the flexure and torsion of cylindrical bars containing some edge and embedded cracks was treated by Sih [16]. The problem was evaluated based on three complex flexure functions including the classical torsion function. Renji and Yulan [17] presented solutions for torsion problems of a circular bar with a rectangular hole and a rectangular bar weekend by an embbeded crack. Li et al. [18] conducted problem of a circular bar containing a polygonal opening and an embedded crack. This portion of the review is related to the torsion problems of bars with rectangular cross section and begins with a study done by Chen [19] who analyzed a rectangular bar with one or two edge cracks perpendicular to the cross section sides. Chen et al. [20] presented a solution for problem of an orthotropic rectangular cross section with an edge crack, bisecting and perpendicular to one boundary of the cross section. Recently, Hassani and Faal [21] focused on study an orthotropic bar with rectangular cross section with aid of the distribution dislocation technique. The bar was under Saint-Venant torsion.

According to the above review, the fracture problem of the shafts under torsion is an interesting problem. It is worth noting that all of the above mentioned works were limited to the shafts with particular orientation and geometry. Also, no paper has been published concerning effect of the coating on the stress intensity factor of the crack tips in the hollow cylinder subjected to torsional loading. Nevertheless, to authors' knowledge, no analytical solution hasn't been presented yet on the Saint-Venant torsion of a hollow cylinder reimforced by an isotropic coating weakened by multiple cracks by considering effect of the coating. In this paper, the closed form solution of the stress fields and warping functions are achieved for a hollow cylinder with isotropic coating containing a Volterra-type screw dislocation (Section 2.1). The torsional rigidity of the cracked shaft with its coating is evaluated in the term of the dislocation density (Section 2.2). The problem is reduced to the solution of a Cauchy singular integral equation. (Section 3). The numerical examples are presented in Section 4 and results are validated by employing available results from the literature. Finally, Section 5 offers concluding remarks.

2- Problem Formulation:

2.1 Dislocation Solution

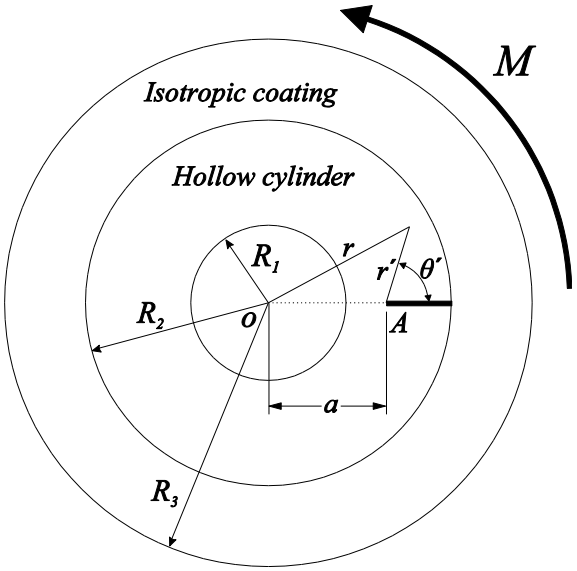

Figure 1. Cross-section of a hollow cylinder with an isotropic coating weakened by a screw dislocation

Consider a prismatic hollow cylinder with an isotropic coating as shown in Fig. 1. R_1 and R_2 are the inner and outer radius of the cylinder, respectively and thickness of the coating is assumed to be R_3-R_2. Considering cylindrical coordinate system, it is assumed that the origin of cylindrical coordinate is located at O and Z-axis is coincided with the axis of the hollow cylinder. The coating is made of an isotropic material, where G are the shear moduli of the coating. A Volterra type screw dislocation, having the Burgers vector b_z, is located at r=a with the line of dislocations in radial direction $(\theta = 0, a \le r \le R_2)$. We divide the whole domain into three regions $R_1 \le r < a$, $a \le r \le R_2$ and $R_2 \le r \le R_3$.

When the shaft is subjected to Saint-Venant torsional loading, components of displacement in the directions of x, y and z axes denoted as u, v and w, respectively, that are given in terms of the angle of twist per unit length of the bar α and of the warping function $\varphi(x, y)$ as [22]

$$\begin{aligned} u &= -\alpha z y \\ v &= \alpha z x \\ w &= \alpha \varphi(x, y) \end{aligned} \tag{1}$$

It is convenient to treat this problem in the cylindrical coordinate system; therefore, the cylindrical transformation is applied to Eqs. (1). Thus, we have

$$\begin{aligned} u_r &= 0 \\ u_\theta &= \alpha r z \\ w &= \alpha \varphi(r, \theta) \end{aligned} \tag{2}$$

The non-vanishing stress components in term of warping function can be expressed as follows

$$\begin{aligned} \tau_{rz} &= \mu\alpha \frac{\partial \varphi(r,\theta)}{\partial r}, \qquad R_1 < r < R_2 \\ \tau_{\theta z} &= \mu\alpha \left(\frac{1}{r} \frac{\partial \varphi(r,\theta)}{\partial \theta} + r \right), \qquad R_1 < r < R_2 \\ \tau_{rz} &= G\alpha \frac{\partial \varphi(r,\theta)}{\partial r}, \qquad R_2 < r < R_3 \\ \tau_{\theta z} &= G\alpha \left(\frac{1}{r} \frac{\partial \varphi(r,\theta)}{\partial \theta} + r \right), \qquad R_2 < r < R_3 \end{aligned} \tag{3}$$

where μ denotes shear modulus in the bar. These stress components must satisfy the equilibrium equation:

$$\frac{\partial \tau_{rz}}{\partial r} + \frac{1}{r} \frac{\partial \tau_{\theta z}}{\partial \theta} + \frac{1}{r} \tau_{rz} = 0$$

we obtain the governing equation of the coating as follows

$$r^2 \frac{\partial^2 \varphi(r,\theta)}{\partial r^2} + r \frac{\partial \varphi(r,\theta)}{\partial r} + \frac{\partial^2 \varphi(r,\theta)}{\partial \theta^2} = 0 \tag{4}$$

The above partial differential equation is solved by means of the finite Fourier sine transform for a regular function $f(r, \theta)$ as

$$F_s(r,n)=\int_0^{\pi} f(r,\theta)\sin(n\theta)\,d\theta \tag{5}$$

The inverse of the finite Fourier sin transform is expressed as

$$f(r,\theta)=\frac{2}{\pi}\sum_{n=1}^{\infty}F_s(r,n)\sin(n\theta) \tag{6}$$

It should be mentioned here that the hollow cylinder and its coating twisted by an applied moment M and then the dislocation cut is made in the cross section of the hollow cylinder.

The boundary condition representing a Volterra-type screw dislocation is

$$\varphi(r,0^+)-\varphi(r,0^-)=\frac{b_z}{\alpha}[H(r-a)-H(r-R_2)] \tag{7}$$

Where $H(.)$ is the Heaviside step function. The continuity of stress components along the dislocation cut requires that

$$\frac{\partial\varphi(r,0^+)}{\partial\theta}=\frac{\partial\varphi(r,0^-)}{\partial\theta} \tag{8}$$

The problem is anti-symmetric with respect to the diameter of the cross section containing the dislocation line, therefore we consider a dislocation solution for the region $0\le\theta\le\pi$ and the boundary conditions (7) and (8) are expressed by

$$\varphi(r,0)=\frac{b_z}{2\alpha}[H(r-a)-H(r-R_2)]$$
$$\varphi(r,\pi)=0 \tag{9}$$

By using the integral transform (6), the partial differential equation (4) can be reduced to the form

$$r^2\frac{\partial^2\Phi_s(r,n)}{\partial r^2}+r\frac{\partial\Phi_s(r,n)}{\partial r}-n^2\Phi_s(r,n)=-\frac{b_z n}{2\alpha}[H(r-a)-H(r-R_1)] \tag{10}$$

The general solution to Eq. (10) can be expressed as

$$\Phi_s(r,n)=A_{1n}r^{-n}+B_{1n}r^{n} \quad for \quad R_1\le r\le a$$
$$\Phi_s(r,n)=A_{2n}r^{n}+B_{2n}r^{-n}+\frac{b_z}{2n\alpha} \quad for \quad a\le r\le R_2 \tag{11}$$
$$\Phi_s(r,n)=A_{3n}r^{n}+B_{3n}r^{-n} \quad for \quad R_2\le r\le R_3$$

According to Eq. (6), the warping function in the whole domain is written as

$$\varphi_1(r,\theta)=\frac{2}{\pi}\sum_{n=1}^{\infty}\left(A_{1n}r^{n}+B_{1n}r^{-n}\right)\sin(n\theta) \quad for \quad R_1\le r\le a$$
$$\varphi_2(r,\theta)=\frac{2}{\pi}\sum_{n=1}^{\infty}\left(A_{2n}r^{n}+B_{2n}r^{-n}+\frac{b_z}{2n\alpha}\right)\sin(n\theta) \quad for \quad a\le r\le R_2 \tag{12}$$
$$\varphi_3(r,\theta)=\frac{2}{\pi}\sum_{n=1}^{\infty}\left(A_{3n}r^{n}+B_{3n}r^{-n}\right)\sin(n\theta) \quad for \quad R_2\le r\le R_3$$

Upon substituting the above relations into the Eq. (6), the warping functions in the whole domain are obtained. Also the stresses are then obtained from Eq. (3) as

$$\tau_{\theta z}(r,\theta)= \frac{2\alpha\mu}{\pi r}\sum_{n=1}^{\infty} n\left(A_{1n}r^{n}+B_{1n}r^{-n}\right)\cos(n\theta) + r\alpha\mu \ , \quad R_1 \le r \le a$$

$$\tau_{\theta z}(r,\theta)= -\frac{b_z\mu}{2nr}+\frac{2\alpha\mu}{\pi r}\sum_{n=1}^{\infty} n\left(A_{2n}r^{n}+B_{2n}r^{-n}\right)\cos(n\theta) + r\alpha\mu \ , \quad a \le r \le R_2$$

$$\tau_{\theta z}(r,\theta)= \frac{2\alpha G}{\pi r}\sum_{n=1}^{\infty} n\left(A_{3n}r^{n}+B_{3n}r^{-n}\right)\cos(n\theta) + r\alpha\mu \ , \quad R_2 \le r \le R_3 \qquad (13)$$

$$\tau_{rz}(r,\theta)=\frac{2\alpha\mu}{\pi r}\sum_{n=1}^{\infty} n\left(A_{1n}r^{n}-B_{1n}r^{-n}\right)\sin(n\theta) \ , \quad R_1 \le r \le a$$

$$\tau_{rz}(r,\theta)=\frac{2\alpha\mu}{\pi r}\sum_{n=1}^{\infty} n\left(A_{2n}r^{n}-B_{2n}r^{-n}\right)\sin(n\theta) \ , \quad a \le r \le R_2$$

$$\tau_{rz}(r,\theta)=\frac{2\alpha G}{\pi r}\sum_{n=1}^{\infty} n\left(A_{3n}r^{n}-B_{3n}r^{-n}\right)\sin(n\theta) \ , \quad R_2 \le r \le R_3$$

where $A_{ln}, B_{ln}, l=1,2,3$ are unknown coefficients which are determined by following boundary and continuity conditions

$$\begin{aligned}
&\tau_{rz}(R_1,\theta)=0\\
&\tau_{rz}(a^{-},\theta)=\tau_{rz}(a^{+},\theta)\\
&\varphi(a^{-},\theta)=\varphi(a^{+},\theta)\\
&\varphi(R_2^{-},\theta)=\varphi(R_2^{+},\theta)\\
&\tau_{rz}(R_2^{-},\theta)=\tau_{rz}(R_2^{+},\theta)\\
&\tau_{rz}(R_3,\theta)=0
\end{aligned} \qquad (14)$$

Application of the conditions (14) to Eqs. (13) and (3) leads to

$$\begin{aligned}
&A_{1n}R_1^{n}-B_{1n}R_1^{-n}=0\\
&A_{1n}a^{n}-B_{1n}a^{-n}=A_{2n}a^{n}-B_{2n}a^{-n}\\
&A_{1n}a^{n}+B_{1n}a^{-n}=A_{2n}a^{n}+B_{2n}a^{-n}+\frac{b_z}{2n\alpha}\\
&\qquad =A_{3n}R_2^{n}+B_{3n}R_2^{-n}\\
&\mu\left(A_{2n}R_2^{n}-B_{2n}R_2^{-n}\right)\\
&\qquad =G_{rz}\left(A_{3n}R_2^{n}-B_{3n}R_2^{-n}\right)\\
&A_{3n}R_3^{n}-B_{3n}R_3^{-n}=0
\end{aligned} \qquad (15)$$

The solution of Eqs. (15) gives:

$$\begin{aligned}
A_{1n}=&-\frac{b_z}{4n\alpha}\Gamma_n\Big[\left(\frac{a\kappa_{23}}{R_2^{2}}\right)^{n}\\
&+\left(C_{eq}-1\right)\left(\left(\kappa_{23}/R_2\right)^{n}-R_2^{-n}\right)\\
&+C_{eq}\left(\left(a/R_2^{2}\right)^{n}-\left(\kappa_{23}/a\right)^{n}\right)-a^{-n}\Big]\\
B_{1n}=&-\frac{b_z}{4n\alpha}\Gamma_n\Big[\left(C_{eq}-1\right)\\
&\left(\left(R_1^{2}\kappa_{23}/R_2\right)^{n}-\left(R_1^{2}/R_2\right)^{n}\right)\\
&+C_{eq}\left(\left(a\kappa_{12}\right)^{n}-\left(R_1^{2}\kappa_{23}/a\right)^{n}\right)\\
&+\left(a\kappa_{12}\kappa_{23}\right)^{n}-\left(R_1^{2}/a\right)^{n}\Big]\\
A_{2n}=&-\frac{b_z}{4n\alpha}\Gamma_n\Big[\left(a\kappa_{23}/R_2^{2}\right)^{n}-\left(\kappa_{12}\kappa_{23}/a\right)^{n}\\
&+C_{eq}\left(\left(a/R_2^{2}\right)^{n}-\left(\kappa_{12}/a\right)^{n}\right)\\
&+\left(1-C_{eq}\right)\left(R_2^{-n}-\left(\kappa_{23}/R_2\right)^{n}\right)\Big]\\
B_{2n}=&-\frac{b_z}{4n\alpha}\Gamma_n\Big[\left(a\kappa_{12}\kappa_{23}\right)^{n}\\
&+\left(C_{eq}-1\right)\left(\left(R_1^{2}\kappa_{23}/R_2\right)^{n}-\left(R_1^{2}/R_2\right)^{n}\right)\\
&-\left(R_1^{2}/a\right)^{n}+C_{eq}\left(\left(a\kappa_{12}\right)^{n}-\left(R_1^{2}\kappa_{23}/a\right)^{n}\right)\Big]\\
&-\frac{b_z}{4n\alpha}a^{n}\\
A_{3n}=&-\frac{b_z\Gamma_n}{\alpha n\left(1-C_{eq}\right)}\begin{pmatrix}\left(aR_2^{G-1}\right)^{n}+\left(\kappa_{12}R_2^{G}\right)^{n}\\-R_2^{-Gn}-\left(R_2^{-G-1}R_1^{2}/a\right)^{n}\end{pmatrix}\\
B_{3n}=&-\frac{b_z\Gamma_n}{\alpha n\left(1-C_{eq}\right)}\begin{pmatrix}\left(aR_2^{G-1}R_3^{2G}\right)^{n}\\+\left(\kappa_{12}R_2^{G}R_3^{2G}\right)^{n}\\-\left(R_2^{-G}R_3^{2G}\right)^{n}\\-\left(R_2^{-G-1}R_1^{2}R_3^{2G}/a\right)^{n}\end{pmatrix}
\end{aligned} \qquad (16)$$

in which:

$$C_{eq}=\frac{\mu-G}{\mu+G}$$

$$\Gamma_n=\frac{1}{1-\kappa_{12}^n\kappa_{23}^n+C_{eq}\left(\kappa_{23}^n-\kappa_{12}^n\right)} \qquad (17)$$

$$\kappa_{12}=\left(\frac{R_1}{R_2}\right)^2$$

$$\kappa_{23}=\left(\frac{R_2}{R_3}\right)^2$$

Upon substituting the above coefficients (16) into the Eqs. (13), the warping functions in the whole domain are obtained. Also the stresses follow from the Eqs. (17) as

$$\tau_{rz}=\frac{b_z\mu}{2\pi r}\sum_{n=1}^{\infty}\Gamma_n\{-\left(ra\kappa_{23}/R_2^2\right)^n+\left(r/a\right)^n+\left(a\kappa_{12}\kappa_{23}/r\right)^n-\left(R_1^2/(ra)\right)^n+C_{eq}\begin{pmatrix}\left(r\kappa_{23}/a\right)^n-\left(ra/R_2^2\right)^n\\+\left(a\kappa_{12}/r\right)^n-\left(R_1^2\kappa_{23}/(ra)\right)^n\end{pmatrix}+\left(C_{eq}-1\right)\begin{pmatrix}\left(R_1^2\kappa_{23}/\left(rR_2\right)\right)^n\\-\left(R_1^2/\left(rR_2\right)\right)^n\\-\left(r\kappa_{23}/R_2\right)^n\\-\left(r/R_2\right)^n\end{pmatrix}\}\sin(n\theta) \qquad (18)$$

$$R_1\le r\le a$$

$$\tau_{\theta z}=-\frac{b_z\mu}{2\pi r}\sum_{n=1}^{\infty}\Gamma_n\{\left(ra\kappa_{23}/R_2^2\right)^n+\left(a\kappa_{12}\kappa_{23}/r\right)^n-\left(r/a\right)^n-\left(R_1^2/ra\right)^n+\left(C_{eq}-1\right)\begin{pmatrix}\left(r\kappa_{23}/R_2\right)^n\\-\left(r/R_2\right)^n\\+\left(R_1^2\kappa_{23}/(rR_2)\right)^n\\-\left(R_1^2/rR_2\right)^n\end{pmatrix}+C_{eq}\begin{pmatrix}\left(a\kappa_{12}/r\right)^n\\-\left(R_1^2\kappa_{23}/(ra)\right)^n\\+\left(ra/R_2^2\right)^n\\-\left(r\kappa_{23}/a\right)^n\end{pmatrix}\}\cos(n\theta)+r\alpha\mu$$

$$R_1\le r\le a$$

$$\tau_{rz}=\frac{b_z\mu}{2\pi r}\sum_{n=1}^{\infty}\Gamma_n\{-\left(r\kappa_{12}\kappa_{23}/a\right)^n-\left(ra\kappa_{23}/R_2^2\right)^n+\left(a\kappa_{12}\kappa_{23}/r\right)^n-\left(R_1^2/ra\right)^n+\left(C_{eq}-1\right)\begin{pmatrix}\left(R_1^2\kappa_{23}/rR_2\right)^n\\-\left(R_1^2/rR_2\right)^n\\+\left(r/R_2\right)^n\\-\left(r\kappa_{23}/R_2\right)^n\end{pmatrix}+\left(a/r\right)^n/\Gamma_n+C_{eq}\begin{pmatrix}\left(a\kappa_{12}/r\right)^n\\-\left(ra/R_2^2\right)^n\\+\left(r\kappa_{12}/a\right)^n\\-\left(R_1^2\kappa_{23}/(ra)\right)^n\end{pmatrix}\}\sin(n\theta)$$

$$a\le r\le R_2$$

$$\tau_{\theta z}=-\frac{b_z\mu}{2\pi r}-\frac{b_z\mu}{2\pi r}\sum_{n=1}^{\infty}\Gamma_n\{\left(ra\kappa_{23}/R_2^2\right)^n-\left(r\kappa_{12}\kappa_{23}/a\right)^n+\left(a\kappa_{12}\kappa_{23}/r\right)^n-\left(R_1^2/ra\right)^n+\left(C_{eq}-1\right)\begin{pmatrix}\left(R_1^2\kappa_{23}/(rR_2)\right)^n\\+\left(r\kappa_{23}/R_2\right)^n\\-\left(r/R_2\right)^n\\-\left(R_1^2/(rR_2)\right)^n\end{pmatrix}+\left(a/r\right)^n/\Gamma_n+C_{eq}\begin{pmatrix}\left(ra/R_2^2\right)^n\\-\left(r\kappa_{12}/a\right)^n\\+\left(R_1^2\kappa_{23}/(ra)\right)^n\\+\left(a\kappa_{12}/r\right)^n\end{pmatrix}\}\cos(n\theta)+r\alpha\mu$$

$$a\le r\le R_2$$

With the aid of the following expansion of Γ_n

$$\Gamma_n = \sum_{m=0}^{\infty}\sum_{i=0}^{m}\sum_{j=0}^{\infty}\frac{C_{eq}^{m}(-1)^{i+m}\Gamma(j+m+1)}{\Gamma(i+1)\Gamma(j+1)\Gamma(-i+m+1)} \quad (19)$$
$$\left(\kappa_{23}^{m-i+j}\kappa_{12}^{j+i}\right)^n$$

the stress components (18) can be summed over the whole domain, leading to

$$\begin{aligned}
&\tau_{rz}(r,\theta) = \frac{b_z\mu}{4\pi r}\sum_{m=0}^{\infty}\sum_{i=0}^{m}\sum_{j=0}^{\infty}\Lambda_{ij}^{m}[\psi_{ij}^{m}\left(\frac{r}{a},\theta\right)\\
&-\psi_{ij}^{m}\left(\frac{ra\kappa_{23}}{R_2^2},\theta\right)\\
&+\psi_{ij}^{m}\left(\frac{a\kappa_{12}\kappa_{13}}{r},\theta\right)\\
&-\psi_{ij}^{m}\left(\frac{R_1^2}{ra},\theta\right)+C_{eq}(\psi_{ij}^{m}\left(\frac{r\kappa_{23}}{a},\theta\right)\\
&-\psi_{ij}^{m}\left(\frac{ra}{R_2^2},\theta\right)+\psi_{ij}^{m}\left(\frac{a\kappa_{12}}{r},\theta\right)\\
&-\psi_{ij}^{m}\left(\frac{R_1^2\kappa_{23}}{ra},\theta\right))\\
&+\left(C_{eq}-1\right)(\psi_{ij}^{m}\left(\frac{R_1^2\kappa_{23}}{rR_2},\theta\right)\\
&-\psi_{ij}^{m}\left(\frac{R_1^2}{rR_2},\theta\right)\\
&+\psi_{ij}^{m}\left(\frac{r}{R_2},\theta\right)-\psi_{ij}^{m}\left(\frac{R_1^2\kappa_{23}}{ra},\theta\right)\Big)]\\
&,R_1<r<a
\end{aligned} \quad (20)$$

$$\begin{aligned}
&\tau_{rz}(r,\theta)\\
&=\frac{b_z\mu}{4\pi r}\sum_{m=0}^{\infty}\sum_{i=0}^{m}\sum_{j=0}^{\infty}\Lambda_{ij}^{m}[\psi_{ij}^{m}\left(\frac{r\kappa_{12}\kappa_{23}}{a},\theta\right)\\
&-\psi_{ij}^{m}\left(\frac{ra\kappa_{23}}{R_2^2},\theta\right)\\
&+\psi_{ij}^{m}\left(\frac{a\kappa_{12}\kappa_{13}}{r},\theta\right)\\
&-\psi_{ij}^{m}\left(\frac{R_1^2}{ra},\theta\right)+C_{eq}(\psi_{ij}^{m}\left(\frac{r\kappa_{12}}{a},\theta\right)\\
&-\psi_{ij}^{m}\left(\frac{ra}{R_2^2},\theta\right)+\psi_{ij}^{m}\left(\frac{a\kappa_{12}}{r},\theta\right)\\
&-\psi_{ij}^{m}\left(\frac{R_1^2\kappa_{23}}{ra},\theta\right)\\
&+\left(C_{eq}-1\right)(\psi_{ij}^{m}\left(\frac{R_1^2\kappa_{23}}{rR_2},\theta\right)\\
&-\psi_{ij}^{m}\left(\frac{R_1^2}{rR_2},\theta\right)+\psi_{ij}^{m}\left(\frac{r}{R_2},\theta\right)\\
&-\psi_{ij}^{m}\left(\frac{r\kappa_{23}}{R_2},\theta\right)\Big)]\\
&+\frac{b_z\mu}{4\pi r}\psi_{00}^{0}\left(\frac{a}{r},\theta\right),a<r<R_2
\end{aligned}$$

$$\begin{aligned}
&\tau_{\theta z}(r,\theta)\\
&=\frac{b_z\mu}{4\pi r}\sum_{m=0}^{\infty}\sum_{i=0}^{m}\sum_{j=0}^{\infty}\Lambda_{ij}^{m}[\phi_{ij}^{m}\left(\frac{ra\kappa_{23}}{R_2^2},\theta\right)\\
&-\phi_{ij}^{m}\left(\frac{r}{a},\theta\right)\\
&+\phi_{ij}^{m}\left(\frac{a\kappa_{12}\kappa_{13}}{r},\theta\right)\\
&-\phi_{ij}^{m}\left(\frac{R_1^2}{ra},\theta\right)\\
&+C_{eq}(\phi_{ij}^{m}\left(\frac{ra}{R_2^2},\theta\right)\\
&-\phi_{ij}^{m}\left(\frac{r\kappa_{23}}{a},\theta\right)+\phi_{ij}^{m}\left(\frac{a\kappa_{12}}{r},\theta\right)\\
&-\phi_{ij}^{m}\left(\frac{R_1^2\kappa_{23}}{ra},\theta\right))\\
&+\left(C_{eq}-1\right)(\phi_{ij}^{m}\left(\frac{R_1^2\kappa_{23}}{rR_2},\theta\right)\\
&-\phi_{ij}^{m}\left(\frac{R_1^2}{rR_2},\theta\right)+\phi_{ij}^{m}\left(\frac{r\kappa_{23}}{R_2},\theta\right)\\
&-\phi_{ij}^{m}\left(\frac{r}{R_2},\theta\right)\Big)]+r\alpha\mu\\
&,R_1<r<a
\end{aligned}$$

$$\tau_{\theta z}\left(r,\theta\right)=-\frac{b_z\mu}{4\pi r}$$
$$+\frac{b_z\mu}{4\pi r}\sum_{m=0}^{\infty}\sum_{i=0}^{m}\sum_{j=0}^{\infty}\Lambda_{ij}^{m}[\phi_{ij}^{m}\left(\frac{ra\kappa_{23}}{R_2^{2}},\theta\right)$$
$$-\phi_{ij}^{m}\left(\frac{r\kappa_{12}\kappa_{23}}{a},\theta\right)$$
$$-\phi_{ij}^{m}\left(\frac{R_1^{2}}{ra},\theta\right)$$
$$+\phi_{ij}^{m}\left(\frac{a\kappa_{12}\kappa_{23}}{r},\theta\right)$$
$$+C_{eq}(\phi_{ij}^{m}\left(\frac{ra}{R_2^{2}},\theta\right)-\phi_{ij}^{m}\left(\frac{r\kappa_{12}}{a},\theta\right)$$
$$+\phi_{ij}^{m}\left(\frac{a\kappa_{12}}{r},\theta\right)$$
$$-\phi_{ij}^{m}\left(\frac{R_1^{2}\kappa_{23}}{ra},\theta\right))$$
$$+\left(C_{eq}-1\right)(\phi_{ij}^{m}\left(\frac{R_1^{2}\kappa_{23}}{rR_2},\theta\right)$$
$$-\phi_{ij}^{m}\left(\frac{R_1^{2}}{rR_2},\theta\right)$$
$$+\phi_{ij}^{m}\left(\frac{r\kappa_{23}}{R_2},\theta\right)$$
$$-\phi_{ij}^{m}\left(\frac{r}{R_2},\theta\right))]$$
$$+\frac{b_z\mu}{4\pi r}\phi_{00}^{0}\left(\frac{a}{r},\theta\right)$$
$$+r\alpha\mu$$
$$,a<r<R_2$$

where

$$\Lambda_{ij}^{m}=\frac{C_{eq}^{m}\left(-1\right)^{i+m}\Gamma\left(j+m+1\right)}{\Gamma\left(i+1\right)\Gamma\left(j+1\right)\Gamma\left(-i+m+1\right)}$$

and

$$\psi_{ij}^{m}\left(x,\theta\right)=\frac{sin\left(\theta\right)}{cosh\left(ln\left(x\,\kappa_{23}^{m-i+j}\kappa_{12}^{j+i}\right)\right)-cos\left(\theta\right)}\qquad(21)$$

$$\phi_{ij}^{m}\left(x,\theta\right)=\frac{sinh\left(ln\left(x\,\kappa_{23}^{m-i+j}\kappa_{12}^{j+i}\right)\right)}{cosh\left(ln\left(x\,\kappa_{23}^{m-i+j}\kappa_{12}^{j+i}\right)\right)-cos\left(\theta\right)}$$

These two functions have features such as the high convergence rate and the convenience of proving Cauchy's singularity, which has led to tensions being rewritten based on two features. In order to verify the stress relationships, the radius of the coating can be considered zero, and the interior radius is assumed to be zero for the purpose of modeling a non-orthogonal bulkhead cylinder. Therefore, solid-state cylindrical stresses without isotropic

$$\tau_{rz}\left(r,\theta\right)=\frac{b_z\mu}{4\pi r}\begin{bmatrix}\psi_{00}^{0}\left(\frac{r}{a},\theta\right)\\-\psi_{00}^{0}\left(\frac{ra}{R_2^{2}},\theta\right)\end{bmatrix}$$
$$,\quad R_1\le r\le a$$
$$\tau_{\theta z}\left(r,\theta\right)=\frac{b_z\mu}{4\pi r}\begin{bmatrix}\phi_{00}^{0}\left(\frac{ra}{R_2^{2}},\theta\right)\\-\phi_{00}^{0}\left(\frac{r}{a},\theta\right)\end{bmatrix}+\alpha G_{\theta z}r$$
$$,\quad R_1\le r\le a\qquad(22)$$
$$\tau_{rz}\left(r,\theta\right)=\frac{b_z\mu}{4\pi r}\begin{bmatrix}\psi_{00}^{0}\left(\frac{a}{r},\theta\right)\\-\psi_{00}^{0}\left(\frac{ra}{R_2^{2}},\theta\right)\end{bmatrix}$$
$$,\quad R_1\le r\le R_2$$
$$\tau_{\theta z}\left(r,\theta\right)=\frac{b_z\mu}{4\pi r}\begin{bmatrix}\phi_{00}^{0}\left(\frac{ra}{R_2^{2}},\theta\right)\\+\phi_{00}^{0}\left(\frac{a}{r},\theta\right)\end{bmatrix}+\alpha G_{\theta z}r$$
$$,\ R_1\le r\le R_2$$

which is exactly the same as that given by Hassani and Faal [13] and this proves the correctness of the derivation of the stress fields in Eq. (20).

To investigate singularity, as shown in Fig (1), a local coordinate is considered at the

dislocation site created at the bar level. The relationship between the local and global coordinate defined is as follows.

$$r = \sqrt{a^2 + (r')^2 + 2ar'\cos\theta'}$$

$$\theta = \sin^{-1}\left(\frac{r'\sin\theta'}{\sqrt{a^2 + (r')^2 + 2ar'\cos\theta'}}\right) \quad (23)$$

$$,\ 0 \le \theta' \le 2\pi$$

Substituting Eq. (23) into Eq. (20) and some manipulations will yield the following results

$$\psi_{ij}^{m}(r/a,\theta) \sim \frac{1}{r'} \ \ as \ \ r' \to 0$$
$$\phi_{ij}^{m}(r/a,\theta) \sim \frac{1}{r'} \ \ as \ \ r' \to 0 \quad (24)$$

2.2 Calculation of torsional rigidity

The torsional rigidity, in cylindrical coordinate, is determined by the following form [22, 23]

$$M = D\alpha = \int_0^{2\pi}\int_0^{R_2} r^2 \tau_{\theta z}(r,\theta)\, dr d\theta \quad (25)$$

in which $\tau_{\theta z}(r,\theta)$ is the stress components given in Eq. (20) and M is the twisting moment to the entire domain. Substituting the Eq. (20) into Eq (25), the torsional rigidity can be written as

$$D = D_0 - \frac{b_z}{2\alpha}\mu\left(R_2^2 - a^2\right) \quad (26)$$

in which

$$D_0 = \frac{\pi}{2}\alpha\begin{pmatrix}\mu\left(R_2^4 - R_1^4\right)\\ +G\left(R_3^4 - R_2^4\right)\end{pmatrix} \quad (27)$$

It is clear from the aforementioned equation that the torsional rigidity has depending on b_z, and D_0 denotes torsional rigidity in the intact hollow cylinder with the isotropic coating.

3. Analyses with multiple cracks

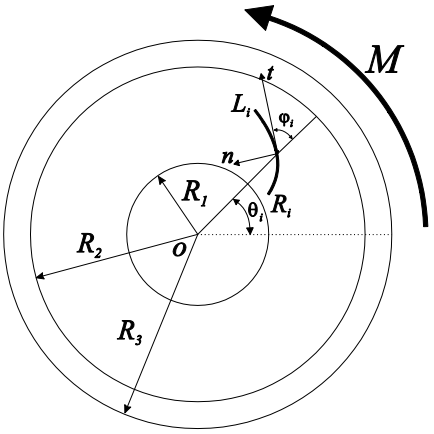

Fig. 2. Cross section of bar with a curved crack

In this section, the dislocation solution performed in the previous section is considered for the analysis of the isotropic coating, weakened by several cracks at this stage, we define a local coordinate system (n,t) attached to the surface of the i th crack (see Fig. 2). The local stress fields on the crack surfaces can be expressed by the following relations

$$\tau_{tz}(r_i,\theta_i) = \tau_{\theta z}(r_i,\theta_i)\sin\varphi_i + \tau_{rz}(r_i,\theta_i)\cos\varphi_i$$
$$\tau_{nz}(r_i,\theta_i) = \tau_{\theta z}(r_i,\theta_i)\cos\varphi_i - \tau_{rz}(r_i,\theta_i)\sin\varphi_i \quad (28)$$

Note that φ_i is the angle between the tangent to the i th crack and radial direction. As an application of the derived dislocation solution we analyze the problem under consideration weekend by multiple cracks. Let dislocations with unknown densities to be distributed on the surface of the i -th crack. By substituting the Eq. (20) into Eq. (28) stress components at a point with coordinate (r_i,θ_i) are achieved. Since the dislocation cut is situated at $\theta = 0$, θ_i is replaced by $\theta_i - \theta_j$ in the local stress fields.

$$
\begin{aligned}
&\tau_{nz}(r_i,\theta)= \\
&\frac{b_z\mu}{4\pi r_i}\{\cos(\phi_i)\sum_{m=0}^{\infty}\sum_{i=0}^{m}\sum_{j=0}^{\infty}\Lambda_{ij}^{m}[\phi_{ij}^{m}\left(\frac{r_i r_j \kappa_{23}}{R_2^2},\theta_i-\theta_j\right) \\
&-\phi_{ij}^{m}\left(\frac{r_i}{r_j},\theta_i-\theta_j\right) \\
&+\phi_{ij}^{m}\left(\frac{r_j\kappa_{12}\kappa_{13}}{r_i},\theta_i-\theta_j\right) \\
&-\phi_{ij}^{m}\left(\frac{R_1^2}{r_i r_j},\theta_i-\theta_j\right) \\
&+C_{eq}(\phi_{ij}^{m}\left(\frac{r_i r_j}{R_2^2},\theta_i-\theta_j\right) \\
&-\phi_{ij}^{m}\left(\frac{r_i\kappa_{23}}{r_j},\theta_i-\theta_j\right) \\
&+\phi_{ij}^{m}\left(\frac{r_j\kappa_{12}}{r_i},\theta_i-\theta_j\right) \\
&-\phi_{ij}^{m}\left(\frac{R_1^2\kappa_{23}}{r_i a},\theta_i-\theta_j\right) \\
&+\left(C_{eq}-1\right)(\phi_{ij}^{m}\left(\frac{R_1^2\kappa_{23}}{r_i R_2},\theta_i-\theta_j\right) \\
&-\phi_{ij}^{m}\left(\frac{R_1^2}{r_i R_2},\theta_i-\theta_j\right) \\
&+\phi_{ij}^{m}\left(\frac{r_i\kappa_{23}}{R_2},\theta_i-\theta_j\right) \\
&-\phi_{ij}^{m}\left(\frac{r_i}{R_2},\theta_i-\theta_j\right)] \\
&-\sin(\phi_i)\sum_{m=0}^{\infty}\sum_{i=0}^{m}\sum_{j=0}^{\infty}\Lambda_{ij}^{m}[\psi_{ij}^{m}\left(\frac{r_i}{r_j},\theta_i-\theta_j\right) \\
&-\psi_{ij}^{m}\left(\frac{r_i r_j\kappa_{23}}{R_2^2},\theta_i-\theta_j\right) \\
&+\psi_{ij}^{m}\left(\frac{a\kappa_{12}\kappa_{13}}{r_i},\theta_i-\theta_j\right) \\
&-\psi_{ij}^{m}\left(\frac{R_1^2}{r_i r_j},\theta_i-\theta_j\right) \\
&+C_{eq}(\psi_{ij}^{m}\left(\frac{r_i\kappa_{23}}{r_j},\theta_i-\theta_j\right) \\
&-\psi_{ij}^{m}\left(\frac{r_i r_j}{R_2^2},\theta_i-\theta_j\right) \\
&+\psi_{ij}^{m}\left(\frac{r_j\kappa_{12}}{r_i},\theta_i-\theta_j\right) \\
&-\psi_{ij}^{m}\left(\frac{R_1^2\kappa_{23}}{r_i a},\theta_i-\theta_j\right)) \\
&+\left(C_{eq}-1\right)(\psi_{ij}^{m}\left(\frac{R_1^2\kappa_{23}}{r_i R_2},\theta_i-\theta_j\right) \\
&-\psi_{ij}^{m}\left(\frac{R_1^2}{r_i R_2},\theta_i-\theta_j\right) \\
&+\psi_{ij}^{m}\left(\frac{r_i}{R_2},\theta_i-\theta_j\right) \\
&-\psi_{ij}^{m}\left(\frac{R_1^2\kappa_{23}}{r_i r_j},\theta_i-\theta_j\right)]\} \\
&,R_1<r_i<r_j
\end{aligned}
\tag{29}
$$

$$
\begin{aligned}
&\tau_{nz}(r_i,\theta_i)= \\
&\frac{b_z\mu}{4\pi r_i}\{\cos(\phi_i)\sum_{m=0}^{\infty}\sum_{i=0}^{m}\sum_{j=0}^{\infty}\Lambda_{ij}^{m}[\phi_{ij}^{m}\left(\frac{r_i r_j\kappa_{23}}{R_2^2},\theta_i-\theta_j\right) \\
&-\phi_{ij}^{m}\left(\frac{R_1^2}{r_i r_j},\theta_i-\theta_j\right) \\
&+\phi_{ij}^{m}\left(\frac{r_j\kappa_{12}\kappa_{23}}{r_i},\theta_i-\theta_j\right) \\
&-\phi_{ij}^{m}\left(\frac{r_i\kappa_{12}\kappa_{23}}{r_j},\theta_i-\theta_j\right) \\
&+C_{eq}(\phi_{ij}^{m}\left(\frac{r_i r_j}{R_2^2},\theta_i-\theta_j\right) \\
&-\phi_{ij}^{m}\left(\frac{r_i\kappa_{12}}{r_j},\theta_i-\theta_j\right) \\
&+\phi_{ij}^{m}\left(\frac{r_j\kappa_{12}}{r_i},\theta_i-\theta_j\right) \\
&-\phi_{ij}^{m}\left(\frac{R_1^2\kappa_{23}}{r_i r_j},\theta_i-\theta_j\right))
\end{aligned}
$$

$$+\left(C_{eq}-1\right)(\phi_{ij}^{m}\left(\frac{R_1^{\,2}\kappa_{23}}{r_i R_2},\theta_i-\theta_j\right)$$
$$-\phi_{ij}^{m}\left(\frac{R_1^{\,2}}{r_i R_2},\theta_i-\theta_j\right)$$
$$+\phi_{ij}^{m}\left(\frac{r_i\kappa_{23}}{R_2},\theta_i-\theta_j\right)$$
$$-\phi_{ij}^{m}\left(\frac{r_i}{R_2},\theta_i-\theta_j\right)])$$
$$+(\phi_{00}^{0}\left(\frac{r_j}{r_i},\theta_i-\theta_j\right)-1)\cos\left(\phi_i\right)$$
$$-\sin\left(\phi_i\right)\sum_{m=0}^{\infty}\sum_{i=0}^{m}\sum_{j=0}^{\infty}\Lambda_{ij}^{m}[\psi_{ij}^{m}\left(\frac{r_i\kappa_{12}\kappa_{23}}{r_j},\theta_i-\theta_j\right)$$
$$-\psi_{ij}^{m}\left(\frac{r_i r_j\kappa_{23}}{R_2^{2}},\theta_i-\theta_j\right)$$
$$+\psi_{ij}^{m}\left(\frac{r_j\kappa_{12}\kappa_{13}}{r_i},\theta_i-\theta_j\right)$$
$$-\psi_{ij}^{m}\left(\frac{R_1^{\,2}}{r_i r_j},\theta_i-\theta_j\right)$$
$$+C_{eq}(\psi_{ij}^{m}\left(\frac{r_i\kappa_{12}}{r_j},\theta_i-\theta_j\right)$$
$$-\psi_{ij}^{m}\left(\frac{r_i r_j}{R_2^{2}},\theta_i-\theta_j\right)$$
$$+\psi_{ij}^{m}\left(\frac{r_j\kappa_{12}}{r_i},\theta_i-\theta_j\right)$$
$$-\psi_{ij}^{m}\left(\frac{R_1^{\,2}\kappa_{23}}{r_i r_j},\theta_i-\theta_j\right)$$
$$+\left(C_{eq}-1\right)(\psi_{ij}^{m}\left(\frac{R_1^{\,2}\kappa_{23}}{r_i R_2},\theta_i-\theta_j\right)$$
$$-\psi_{ij}^{m}\left(\frac{R_1^{\,2}}{r_i R_2},\theta_i-\theta_j\right)$$
$$+\psi_{ij}^{m}\left(\frac{r_i}{R_2},\theta_i-\theta_j\right)$$
$$-\psi_{ij}^{m}\left(\frac{r_i\kappa_{23}}{R_2},\theta_i-\theta_j\right)])$$
$$-\psi_{00}^{0}\left(\frac{r_j}{r_i},\theta_i-\theta_j\right)\sin\left(\phi_i\right)\}$$
$$+r_i\alpha\mu\cos\left(\phi_i\right),r_j<r_i<R_2$$

Now, resultant traction on the crack surface due to the distribution dislocations may thus be obtained by integration of above equations with respect to the normalized crack length. In the following discussion, $\alpha=M/D$, is substituted in the Eq. (29). The stress free condition of the crack surfaces can be applied to obtain a set of integral equations by separating the terms without b_z, as follow

$$Q_i\left(r_i(s),\theta_i(s)\right)=\sum_{j=1}^{N}\int_{-1}^{1}k_{ij}(s,t)b_{zj}(t)dt \qquad (30)$$
$$,-1\le s\le 1$$
$$,\ i=1,2,\ldots,N$$

The left side of the integral equation (26) is $Q_i(s)=-\frac{M}{D_0}\mu r_i\cos\varphi_i$ and $k_{ij}(s,t)$ is described in the Appendix.

It is clear that the integral equations (30) must be evaluated under the following single-valuedness condition

$$\int_{-1}^{1}b_{zj}(t)\,d\lambda_j=0 \qquad (31)$$

in which $d\lambda_j=\sqrt{[r_j'(t)]^2+[r_j(t)\theta_j'(t)]^2}dt$ denotes the infinitesimal segment on the surface of j-th crack.

For embedded cracks the Cauchy singular integral Equations (30) and (31) should be solved simultaneously to determine unknown dislocation density on the cracks surfaces. The numerical solution of these equations is carried out by the technique

developed by Faal et al. [24]. The stress fields exhibit square-root singularity at crack tips. Therefore, the dislocation densities for embedded and edge cracks are taken as

$$b_{zj}(t)=\frac{g_{zj}(t)}{\sqrt{1-t^2}}\ ,\ -1\le t\le 1 \quad \textit{for embedded cracks} \tag{32}$$

$$b_{zj}(t)=g_{zj}(t)\sqrt{\frac{1-t}{1+t}}\ ,\ -1\le t\le 1 \quad \textit{for edge cracks}$$

With aid of the $\alpha=M/D$ and some manipulations the torsional rigidity in the hollow cylinder with the orthotropic coating can be calculated by the following formula

$$D=\frac{D_0}{1+\frac{\mu}{2M}\sum_{j=1}^{N}\int_{-1}^{1}[R_2^2-\left(r_j(t)\right)^2]\sqrt{\left[r_j'(t)\right]^2+\left[r_j\theta_j'(t)\right]^2}\,b_{zj}(t)dt} \tag{33}$$

where N denotes the number of the cracks. The determination of the torsional rigidity is based on discretizing the domain of the integral appeared in Eq. (33) at m discrete points $t_k=\cos(\pi(2k-1)/(2m)),k=1,2,\ldots,m$.

Thus, the torsional rigidity is found to be

$$D=\frac{D_0}{1+\frac{\pi\mu}{2Mm}\sum_{j=1}^{N}\sum_{k=1}^{m}[R_2^2-\left(r_j(t_k)\right)^2]\sqrt{\left[r_j'(t_k)\right]^2+\left[r_j\theta_j'(t_k)\right]^2}\,g_{zj}(t_k)\Phi(t_k)} \tag{34}$$

where

$$\Phi(t_k)=\begin{cases}1 & \textit{for embedded cracks}\\ 1-t_k & \textit{for edge cracks}\end{cases} \tag{35}$$

After calculating $g_{zj}(t)$, stress intensity factors for the cracks were derived by Faal and Fariborz [24]. These are

$$\begin{cases}k_{IIILi}=\\ \frac{\sqrt{\pi}}{2}\mu\left[\begin{matrix}\left(r_i'(-1)\right)^2\\ +\left(r_i(-1)\theta_i'(-1)\right)^2\end{matrix}\right]^{\frac{1}{4}}g_{zi}(-1)\\ k_{IIIRi}=\\ -\frac{\sqrt{\pi}}{2}\mu\left[\begin{matrix}\left(r_i'(1)\right)^2\\ +\left(r_i(1)\theta_i'(1)\right)^2\end{matrix}\right]^{\frac{1}{4}}g_{zi}(1)\\ \textit{for embedded cracks}\end{cases} \tag{36}$$

$$k_{IIIi}=\sqrt{\pi}\mu\left[\begin{matrix}\left(r_i'(-1)\right)^2\\ +\left(r_i(-1)\theta_i'(-1)\right)^2\end{matrix}\right]^{\frac{1}{4}}g_{zi}(-1)$$

for edge cracks

4. Numerical Results

In this section, several numerical examples are presented to prove the correctness of the dislocation method to show the capability of the current approach in handling problems containing several cracks. The torsional problem of a hollow cylinder with an isotropic layer involved multiple radial cracks hasn't been studied by other investigators, yet. In the lack of similar studies, the validation is only allocated to the papers relating to cracked shafts without isotropic layer subjected to the torsional loading. We use a dimensionless parameter $\frac{\mu}{G}=0.5$ evaluate effect of the coating on the stress intensity factors. In the numerical examples the dimensionless stress intensity factors, k_{III}/k_0, will be considered in which $k_0=\mu M_0 R_2\sqrt{\pi l}/J_0$. Also, l refers to a half-length of embedded crack. The effect of the coating will be discussed with $R_3-R_2=0.1R_2$.

Example 1.

The first example is allocated to a bar weakened by a straight radial crack. Firstly, by taking this problem as a bar without any coating, i.e. $R_2 = R_3$, the numerical solution will be compared with existing results to show accuracy and efficiency of the dislocation method. The center of the radial crack is located at $r_0 = 0.3R_2$. The results of dislocation method are compared with results of the reference [25]. The results show negligible difference between the results of the present work and those obtained by Tao and Tang [25]. The indexes i and o designate to the inner and outer tips of the crack. The normalized stress intensity factors and the normalized torsional rigidities have been compared with existing results in the reference [25] in Table. 1.

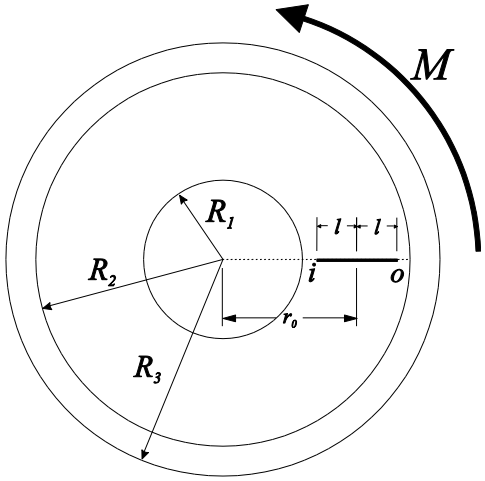

Fig 3. Hollow cylinder cross section with one embedded radial crack

In the following, an isotropic coating as an actuator with thickness $t = 0.1R_2$ is considered. The hollow cylinder is weakened by a straight crack by setting $l = 0.3R_2$ and $r_0 = 0.4R_2$.

Table.1. Comparison between the numerical results of the present study and the results of the reference [25] for a radial crack.

l / R	J / J_0		k_{IIIi} / k_0		k_{IIIo} / k_0	
	Present study	Reference [25]	Present study	Reference [25]	Present study	Reference [25]
0.1	0.9982	0.9981	0.2522	0.2518	0.3525	0.3519
0.2	0.9922	0.9922	0.2087	0.2070	0.4113	0.4081
0.3	0.9808	0.9808	0.1695	0.1660	0.4796	0.4703
0.4	0.9612	0.9612	0.1352	0.1295	0.5650	0.5427

The effect of thickness of the coating on the stress intensity factor has been illustrated in Fig 4. The center of the crack has been situated at $r_0 = 0.5R_2$ and half-length of the crack is $l = 0.1R_2$ .As we expected, as the radius of coating goes up, the dimensionless stress intensity factor for each crack tip decreases. This phenomenon helps reinforcement of the structure.

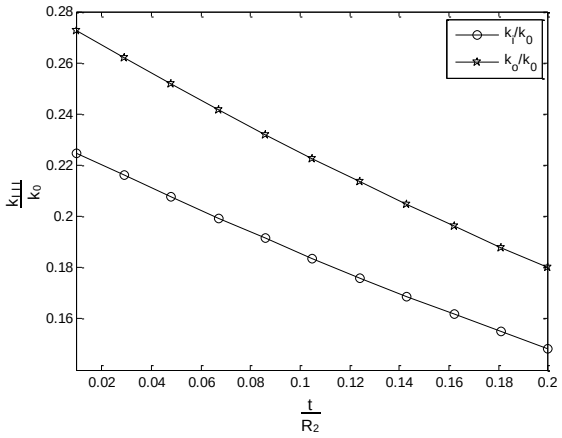

Fig 4. Variation of the dimensionless stress intensity factor against normalized thickness for a straight radial crack.

In the following discussion, the variations of dimensionless stress intensity factor and torsional rigidity versus the half crack length have been illustrated in Fig. 5 and 6. The stress intensity factor for the crack tip i must be gone up with increasing the crack length. However, the stress intensity factor declines because the crack tip i

approaches to stress free surface. In addition, we observe a normal trend at the crack tip o for the variations of stress intensity factor. As expected, the dimensionless torsional rigidity is decreased by increasing the length of the crack which makes a weaker cross section.

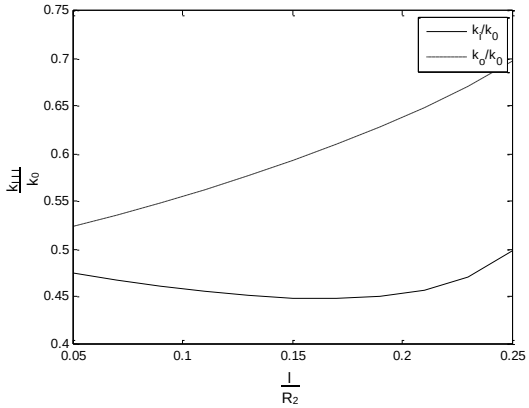

Fig 5. Variation of the dimensionless stress intensity factor against the normalized half crack length for a straight radial crack.

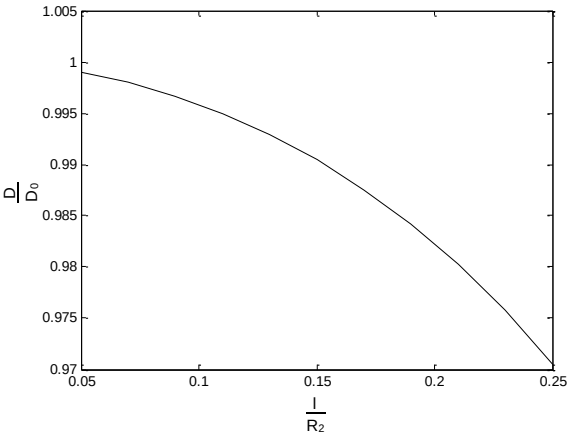

Fig 6. Variation of the dimensionless torsional against normalized half crack length for a straight radial crack.

Example 3.

In the third example, consider a hollow cylinder with an isotropic layer weakened by one embedded crack perpendicular to the radial direction. The center of the crack has been situated at the distance of $d = 0.5R_2$ from the origin of the cylindrical coordinate, and length of the crack has considered $l = 0.1R_2$, as shown in Fig 15.

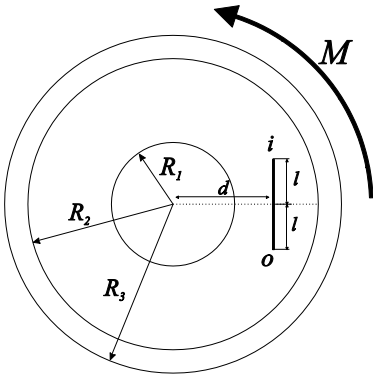

Fig 7. Hollow cylinder cross section with one embedded crack normal to the radial direction

In the first plot of this example, the variations of the dimensionless stress intensity factors as a function of dimensionless coating thickness have been evaluated for $r_0 = 0.5R_2$ and $l = 0.2R_2$ (Fig 8). According to the trend of the previous examples, stress intensity factors decrease as the isotropic layer becomes thicker.

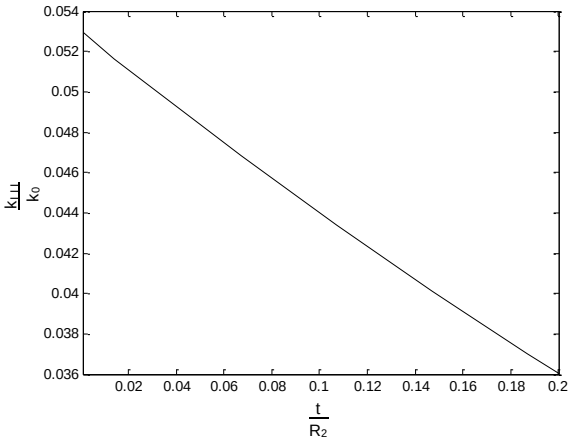

Fig. 8. The graph of the normalized stress intensity factor with normalized coating thickness

In the following discussion, the variation of dimensionless stress intensity factors and torsional rigidity have been illustrated as a function of the dimensionless half crack length in Fig 9 and 10, respectively. As expected, the dimensionless stress intensity factor at the crack tips is gone up by increasing of the crack length. The

dimensionless torsional rigidity goes down as the crack length increases and this makes a weaker bar.

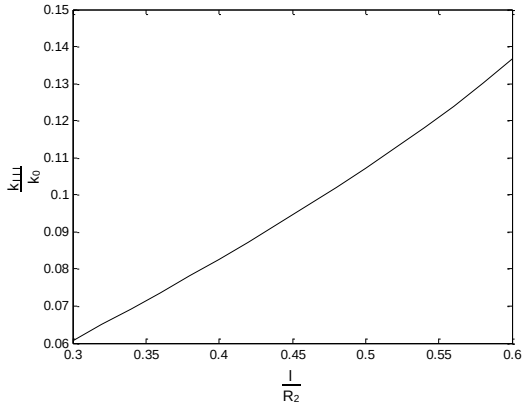

Fig. 9. The graph of normalized stress intensity factors against normalized half crack length

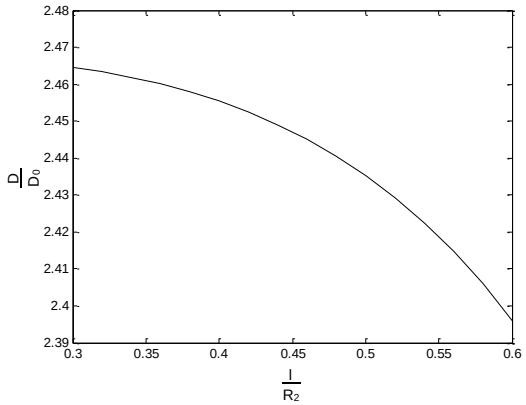

Fig. 10. The graph of normalized torsional rigidity against normalized half crack length

Example 3.

In the next example, a hollow cylinder with an isotropic coating containing two inclined cracks is considered. The crack lengths are assumed equal and each crack tip is located on the circle $a = 0.75R_2$. In the other words, both of the cracks are a part of the chord with the central angle $\pi/4$ as shown in Fig 11.

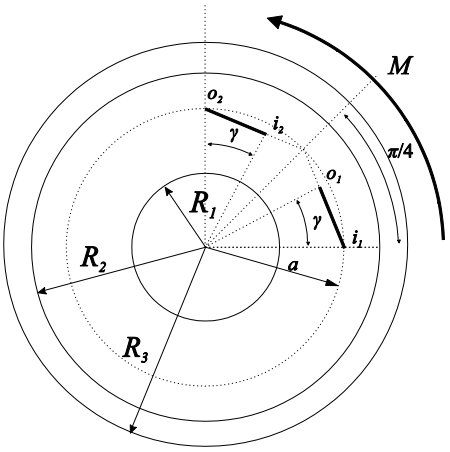

Fig 11. Cross section of a hollow cylinder with two inclined cracks

In the continuation of the example, we want to evaluate the effect of the effective coating thickness on the stress intensity factors by setting $l = 0.3R_2$. Hence, the variation of dimensionless stress intensity factors as a function of the dimensionless half length of the cracks for each of the crack tips can be seen in Fig 12 and it shows same trend of previous examples.

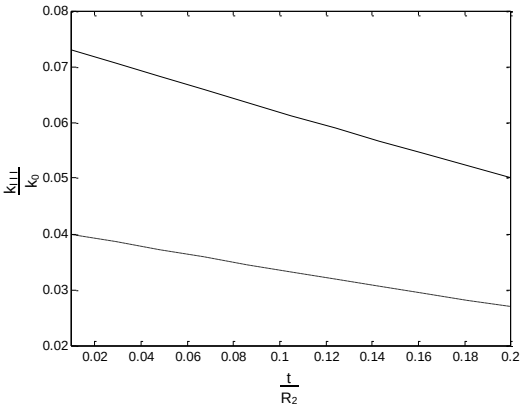

Fig. 12. Variation of normalized stress intensity factors against normalized coating thickness

In the next part of this example, we evaluate the effect of crack length on the stress intensity factor and torsional rigidity in Fig 13 and 14, respectively. The stress intensity factors must be gone up by growing the cracks because of interaction between the cracks. However, there is a decrease for the stress intensity factor at crack tip o_1 since this tip approaches to the

stress free surface. Also, the torsional rigidity falls down by growing the cracks.

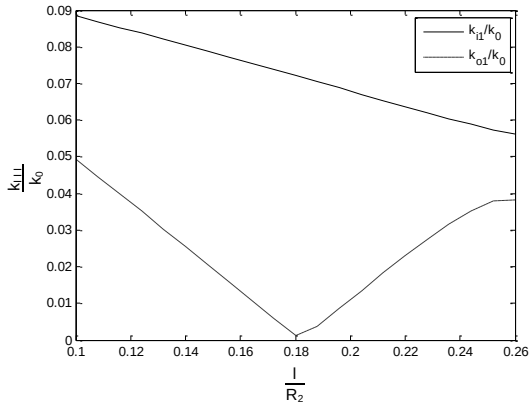

Fig. 13. Graph of normalized stress intensity factors against normalized half crack length

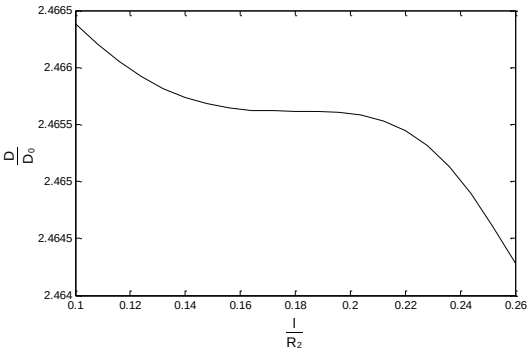

Fig. 14. Graph of normalized torsional rigidity against normalized half crack length

Example 5.

In the final example, consider a hollow cylindrical shaft with an effective coating layer weakened by one straight crack normal to the radial direction and one eccentric crack, as shown in Fig 15. The length of the straight crack is constant and it is considered $l_1 = 0.5R_2$. The distance between center of the straight crack and center of the domain is $d = 0.4R_2$. The center of the eccentric crack is fixed at distance of $e = 0.2R_2$ from the center of the bar and its radius is assumed $a = 0.5R_2$. The effect of coating thickness has been considered and decrease in the normalized stress intensity factors with growing coating thickness is realized in Fig 16.

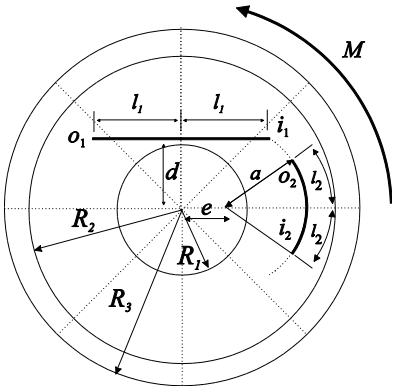

Fig 15. Cross section of a hollow cylinder with two cracks

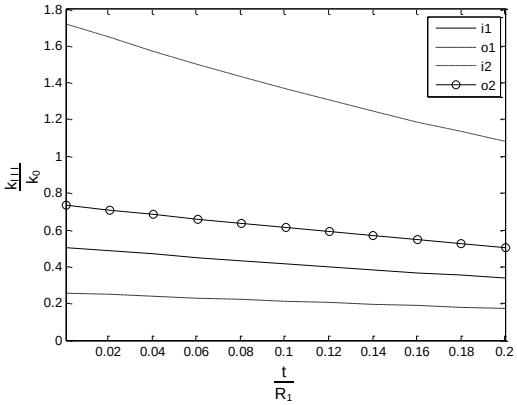

Fig. 16. Graph of normalized stress intensity factors against normalized thickness

The variation of the dimensionless stress intensity factors against the length of the eccentric crack, l_2 / R_2, can be seen in Fig. 17. There is a slight decrease in the stress intensity factor for the crack tip i_1 since it recedes from crack tip i_2 by growing the circular crack. After that stress intensity factor for the crack tip i_1 rises dramatically, because there is interaction between the tips of the cracks. The crack tip o_1 recedes from crack tip i_2 and it approaches to crack tip o_2 as the length of the eccentric crack increases. The stress intensity factor at crack tip o_2 remains steady because of a compromise between two different effects. As expected, the dimensionless stress intensity factor at the crack tip i_2 goes up with the circular crack

growth. The stress intensity factor of the crack tip o_2 reduces at beginning of the graph. Then it rises by increasing length of the circular crack because of interaction between the crack tips o_2 and i_1. Fig. 18 illustrates the effect of the crack length on the torsional rigidity. The torsional rigidity of the bar is decreased with the crack length growth which makes a weaker domain.

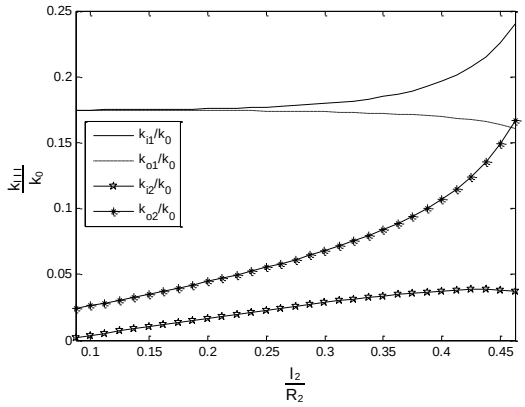

Fig. 17. The graph of the dimensionless stress intensity factors against dimensionless half length of the circular crack l_2 / R_2

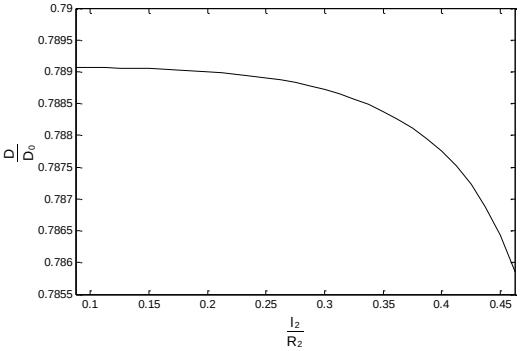

Fig. 18. The graph of the dimensionless torsional rigidity against dimensionless half length of the circular crack l_2 / R_2

5. Conclusion

This work presented an efficient dislocation approach for the evaluation of the stress intensity factors for multiple arbitrarily shaped cracks in a hollow circular bar with an isotropic coating. A solution of the torsion problem of a hollow circular bar with an isotropic coating weakened by Volterra-type dislocation was first presented in terms of dislocation density. The problem was reduced to a set of singular integral equations of Cauchy singular type in the rectangular cross section, by using the distribution dislocation technique to analyze the problem with multiple smooth cracks. The integral equations were solved numerically by reducing them to a system of algebraic equations. Finally, the stress intensity factor for the crack tips and the torsional rigidity of the domain under consideration were evaluated. To summarize, the stress intensity factors of crack tips and torsional rigidity in the cross section with the isotropic coating were found to depend on critical factors such as the distance of the crack tip from the free boundary of the domain, thickness of the coating, crack length and the interaction between the cracks.

Appendix

Kernels of Eq .(30) are:

$$
\begin{aligned}
&k_{ij}(s,t) = \\
&-\frac{\mu}{4\pi r_i(s)}\{\sin(\phi_i(s))\sum_{m=0}^{\infty}\sum_{i=0}^{m}\sum_{j=0}^{\infty}\Lambda_{ij}^{m}((C_{eq}+1) \\
&(-\psi_{ij}^{m}\left(\frac{r_i(s)r_j(t)}{R_2^2},(\theta_i(s)-\theta_j(t))\right) \\
&+\psi_{ij}^{m}\left(\frac{r_i(s)}{r_j(t)},\theta_i(s)-\theta_j(t)\right) \\
&+\psi_{ij}^{m}\left(\frac{r_j(t)}{r_i(s)}\kappa_{12}\kappa_{23},\theta_i(s)-\theta_j(t)\right) \\
&-\psi_{ij}^{m}\left(\frac{R_1^2}{r_i(s)r_j(t)},\theta_i(s)-\theta_j(t)\right))
\end{aligned}
$$

$$+\left(C_{eq}-1\right)(-\psi_{ij}^{m}\left(\frac{r_i(s)r_j(t)}{R_2^2},\theta_i(s)-\theta_j(t)\right)$$
$$+\psi_{ij}^{m}\left(\frac{r_i(s)}{r_j(t)}\kappa_{23},\theta_i(s)-\theta_j(t)\right)$$
$$-\psi_{ij}^{m}\left(\frac{R_1^2}{r_i(s)r_j(t)}\kappa_{23},\theta_i(s)-\theta_j(t)\right))$$
$$+2(-\psi_{ij}^{m}\left(\frac{r_i(s)}{R_2},\theta_i(s)-\theta_j(t)\right)$$
$$+\psi_{ij}^{m}\left(\frac{r_i(s)}{R_2}\kappa_{23},\theta_i(s)-\theta_j(t)\right)$$
$$-\psi_{ij}^{m}\left(\frac{r_j(t)}{r_i(s)}\kappa_{12},\theta_i(s)-\theta_j(t)\right)$$
$$+\psi_{ij}^{m}\left(\frac{R_1^2}{r_i(s)R_2},\theta_i(s)-\theta_j(t)\right)$$
$$-\psi_{ij}^{m}\left(\frac{R_1^2}{r_i(s)R_2}\kappa_{23},\theta_i(s)-\theta_j(t)\right))$$
$$-\cos\left(\phi_i(s)\right)\sum_{m=0}^{\infty}\sum_{i=0}^{m}\sum_{j=0}^{\infty}\Lambda_{ij}^{m}((C_{eq}+1)$$
$$(-\phi_{ij}^{m}\left(\frac{r_i(s)r_j(t)}{R_2^2}\kappa_{23},\theta_i(s)-\theta_j(t)\right)$$
$$+\phi_{ij}^{m}\left(\frac{r_i(s)}{r_j(t)},\theta_i(s)-\theta_j(t)\right)$$
$$+\phi_{ij}^{m}\left(\frac{R_1^2}{r_i(s)r_j(t)},\theta_i(s)-\theta_j(t)\right)$$
$$-\phi_{ij}^{m}\left(\frac{r_j(t)}{r_i(s)}\kappa_{12}\kappa_{23},\theta_i(s)-\theta_j(t)\right))+$$
$$\left(C_{eq}-1\right)(-\phi_{ij}^{m}\left(\frac{r_i(s)r_j(t)}{R_2^2},\theta_i(s)-\theta_j(t)\right)$$
$$+\phi_{ij}^{m}\left(\frac{r_i(s)}{r_j(t)}\kappa_{23},\theta_i(s)-\theta_j(t)\right)$$
$$-\phi_{ij}^{m}\left(\frac{r_j(t)}{r_i(s)}\kappa_{12},\theta_i(s)-\theta_j(t)\right)$$
$$+\phi_{ij}^{m}\left(\frac{R_1^2}{r_i(s)r_j(t)}\kappa_{23},\theta_i(s)-\theta_j(t)\right))$$
$$+2(\phi_{ij}^{m}\left(\frac{r_i(s)}{R_2},\theta_i(s)-\theta_j(t)\right)$$
$$-\phi_{ij}^{m}\left(\frac{r_i(s)}{R_2}\kappa_{23},\theta_i(s)-\theta_j(t)\right)$$
$$-\phi_{ij}^{m}\left(\frac{R_1^2}{r_i(s)R_2},\theta_i(s)-\theta_j(t)\right)$$
$$+\phi_{ij}^{m}\left(\frac{R_1^2}{r_i(s)R_2}\kappa_{23},\theta_i(s)-\theta_j(t)\right))\}$$
$$,R_1<r_i(s)<r_j(t)$$
$$k_{ij}(s,t)=\frac{\mu b_z}{4\pi r_i(s)}\begin{pmatrix}-\cos\left(\phi_i(s)\right)\\+\phi_{00}^{0}\begin{pmatrix}\frac{r_j(t)}{r_i(s)}\\,\theta_i(s)-\theta_j(t)\end{pmatrix}\cos\left(\phi_i(s)\right)\end{pmatrix}$$
$$-\psi_{00}^{0}\left(\frac{r_j(t)}{r_i(s)},\theta_i(s)-\theta_j(t)\right)\sin\left(\phi_i(s)\right))$$
$$+\frac{\mu b_z}{4\pi r_i(s)}\{\cos\left(\phi_i(s)\right)\sum_{m=0}^{\infty}\sum_{i=0}^{m}\sum_{j=0}^{\infty}\Lambda_{ij}^{m}(\phi_{ij}^{m}$$
$$\left(\frac{r_i(s)r_j(t)}{R_2^2}\kappa_{23},\theta_i(s)-\theta_j(t)\right)$$
$$-\phi_{ij}^{m}\left(\frac{r_i(s)}{r_j(t)}\kappa_{12}\kappa_{23},\theta_i(s)-\theta_j(t)\right)$$
$$+\phi_{ij}^{m}\left(\frac{r_j(t)}{r_i(s)}\kappa_{12}\kappa_{23},\theta_i(s)-\theta_j(t)\right)$$
$$-\phi_{ij}^{m}\left(\frac{R_1^2}{r_i(s)r_j(t)},\theta_i(s)-\theta_j(t)\right))$$
$$+\left(C_{eq}-1\right)(\phi_{ij}^{m}\left(\frac{r_i(s)r_j}{R_2^2},\theta_i(s)-\theta_j(t)\right)$$
$$-\phi_{ij}^{m}\left(\frac{r_i(s)}{r_j(t)}\kappa_{12},\theta_i(s)-\theta_j(t)\right)$$
$$+\phi_{ij}^{m}\left(\frac{r_j(t)}{r_i(s)}\kappa_{12},\theta_i(s)-\theta_j(t)\right)$$

$$-\phi_{ij}^{m}\left(\frac{R_1^2}{r_j(t)}\kappa_{23},\theta_i(s)-\theta_j(t)\right))$$
$$+2(\phi_{ij}^{m}\left(\frac{r_i(s)}{R_2},\theta_i(s)-\theta_j(t)\right)$$
$$-\phi_{ij}^{m}\left(\frac{r_j(t)}{r_i(s)}\kappa_{12},\theta_i(s)-\theta_j(t)\right)$$
$$-\theta_j\left(\frac{R_1^2}{r_i(s)R_2},\theta_i(s)-\theta_j(t)\right)$$
$$-\phi_{ij}^{m}\left(\frac{R_1^2}{r_i(s)R_2}\kappa_{23},\theta_i(s)-\theta_j(t)\right))$$
$$+\psi_{ij}^{m}\left(\frac{r_i(s)}{r_j(t)}\kappa_{12}\kappa_{23},\theta_i(s)-\theta_j(t)\right)$$
$$+\psi_{ij}^{m}\left(\frac{r_j(t)}{r_i(s)}\kappa_{12}\kappa_{23},\theta_i(s)-\theta_j(t)\right))$$
$$-\psi_{ij}^{m}\left(\frac{R_1^2}{r_i(s)r_j(t)},\theta_i(s)-\theta_j(t)\right)$$
$$+\left(C_{eq}-1\right)(-\psi_{ij}^{m}\left(\frac{r_i(s)r_j}{R_2^2},\theta_i(s)-\theta_j(t)\right)$$
$$+\psi_{ij}^{m}\left(\frac{r_i(s)}{r_j(t)}\kappa_{12},\theta_i(s)-\theta_j(t)\right)$$
$$+\psi_{ij}^{m}\left(\frac{r_j(t)}{r_i(s)}\kappa_{12},\theta_i(s)-\theta_j(t)\right)$$
$$-\psi_{ij}^{m}\left(\frac{R_1^2}{r_i(s)r_j(t)}\kappa_{23},\theta_i(s)-\theta_j(t)\right))$$
$$+2(-\psi_{ij}^{m}\left(\frac{r_i(s)}{R_2},\theta_i(s)-\theta_j(t)\right)$$
$$+\psi_{ij}^{m}\left(\frac{R_1^2}{r_i(s)R_2},\theta_i(s)-\theta_j(t)\right)$$
$$-\psi_{ij}^{m}\left(\frac{R_1^2}{r_i(s)R_2}\kappa_{23},\theta_i(s)-\theta_j(t)\right)))\}$$
$$,\ r_j(t)<r_i(s)<R_2$$

References

[1] ECSEDI, I. and BAKSA, A. Prandtl's formulation for the Saint–Venant's torsion of homogeneous piezoelectric beams, *International Journal of Solids and Structures*, **47**, 3076-3083, (2010).

[2] ECSEDI, I. Elliptic cross section without warping under torsion, *Mechanics Research Communications*, **31**, 147-150, (2004).

[3] RONGQIAO, X., JIANSHENG, H. and WEIQIU, C. Saint-Venant torsion of orthotropic bars with inhomogeneous rectangular cross section, *Composite Structures*, **92**, 1449-1457, (2010).

[4] BASSALI, W.A. and OBAID, S.A. On the Torsion of Elastic Cylindrical Bars, *ZAMM - Journal of Applied Mathematics and Mechanics / Zeitschrift für Angewandte Mathematik und Mechanik*, **61**, 639-650, (1981).

[5] LEBEDEV, N.I.N., SKALSKAYA, I.P., UFLAND, I.A.S. and SILVERMAN, R.A., Worked Problems in Applied Mathematics, Dover Publications 1979.

[6] XIAO-CHUN, W. and REN-JI, T. On the torsion of a cylinder with several cracks, *Applied Mathematics and Mechanics*, **9**, 745-754, (1988).

[7] KARIMI, M., ATRIAN, A., GHASSEMI, A. and VAHABI, M. Torsion analysis of a hollow cylinder with an orthotropic coating weakened by multiple cracks, *Theoretical and Applied Fracture Mechanics*, **90**, 110-121, (2017).

[8] WANG, Y.-B. and LU, Z.-Z. New boundary element method for torsion problems of cylinder with curvilinear cracks, *Applied Mathematics and Mechanics*, **26**, 1531-1538, (2005).

[9] CHEN, Y.Z. Multiple crack problems for torsion thin-walled cylinder, *International Journal of Pressure Vessels and Piping*, **76**, 49-53, (1999).

[10] TWEED, J. and ROOKE, D.P. The torsion of a circular cylinder containing a symmetric array of edge cracks, *International*

Journal of Engineering Science, **10**, 801-812, (1972).

[11] YUANHAN, W. Torsion of a thick-walled cylinder with an external crack: boundary collocation method, *Theoretical and Applied Fracture Mechanics*, **14**, 267-273, (1990).

[12] CHEN, J.T., CHEN, K.H., YEIH, W. and SHIEH, N.C. Dual boundary element analysis for cracked bars under torsion, *Engineering Computations*, **15**, 732-749, (1998).

[13] HASSANI, A.R. and FAAL, R.T. Saint-Venant torsion of orthotropic bars with a circular cross-section containing multiple cracks, *Mathematics and Mechanics of Solids*, **21**, 1198-1214, (2014).

[14] YI-ZHOU, C. On the torsional rigidity for a hollow shaft with outer or inner keys, *Computer Methods in Applied Mechanics and Engineering*, **42**, 107-118, (1984).

[15] FANG-MING, T. and REN-JI, T. Saint-Venant's torsion problem for a composite circular cylinder with aninternal edge crack, *Applied Mathematics and Mechanics*, **14**, 507-516, (1993).

[16] SIH, G.C. Strength of Stress Singularities at Crack Tips for Flexural and Torsional Problems, *Journal of Applied Mechanics*, **30**, 419-425, (1963).

[17] RENJI, T. and YULAN, L. Torsion problems for a cylinder with a rectangular hole and a rectangular cylinder with a crack, *Acta Mechanica Sinica*, **8**, 165-172, (1992).

[18] LI, Y.L., HU, S.Y. and TANG, R.J. Interaction of crack-tip and notch-tip stress singularities for circular cylinder in torsion, *Theoretical and Applied Fracture Mechanics*, **18**, 259-272, (1993).

[19] CHEN, Y.-Z. Solutions of torsion crack problems of a rectangular bar by harmonic function continuation technique, *Engineering Fracture Mechanics*, **13**, 193-212, (1980).

[20] CHEN, Y.Z., LIN, X.Y. and CHEN, R.S. Solution of torsion crack problem of an orthotropic rectangular bar by using computing compliance method, *Communications in Numerical Methods in Engineering*, **13**, 655-663, (1997).

[21] HASSANI, A.R. and FAAL, R.T. Saint-Venant torsion of orthotropic bars with rectangular cross section weakened by cracks, *International Journal of Solids and Structures*, **52**, 165-179, (2015).

[22] BARBER, J.R., Elasticity, Springer 2009.

[23] HASSANI, A.R. and FAAL, R.T. Torsion analysis of cracked circular bars actuated by a piezoelectric coating, *Smart Materials and Structures*, **25**, 125030, (2016).

[24] FAAL, R.T., FARIBORZ, S.J. and DAGHYANI, H.R. Antiplane deformation of orthotropic strips with multiple defects, *Journal of Mechanics of Materials and Structures*, **1**, 1097-1114, (2006).

[25] TAO, F.M. and TANG, R.J. Saint-Venant's torsion problem for a composite circular cylinder with aninternal edge crack, *Applied Mathematics and Mechanics*, **14**, 507-516, (1993).